Mon. Not. R. Astron. Soc. **286,** 436–446 (1997)

A magnetic propeller in the cataclysmic variable AE Aquarii

Graham A. Wynn,[1]★ Andrew R. King[1] and Keith Horne[2]

[1]*Astronomy Group, Leicester University, University Road, Leicester LE1 7RH*
[2]*Department of Physics and Astronomy, University of St Andrews, North Haugh, St Andrews KY16 9SS*

Accepted 1996 November 12. Received 1996 October 31; in original form 1996 June 19

ABSTRACT

Current treatments of accretion flows in magnetic cataclysmic variables (CVs) imply that the criterion for disc formation depends only on the accretion rate and the magnetic field strength, and is independent of the spin rate of the accreting star. The low accretion rate in the moderately magnetic CV AE Aqr should allow disc formation, yet the single-peaked Balmer emission lines show no evidence of a disc. We interpret these data as evidence that the rapidly rotating white dwarf in AE Aqr ejects most of the matter transferred from the secondary. The possibility of such states was pointed out in earlier theoretical work modelling the gas flow as inhomogeneous and diamagnetic. Explicit application of this model to AE Aqr accounts for the observed spin-down of the white dwarf, and gives estimates of the white dwarf magnetic moment and the mass transfer rate as $\sim 10^{32}$ G cm^3 and $\gtrsim 10^{17}$ g s^{-1} respectively. We show that AE Aqr is likely to alternate between phases of disc accretion, in which the white dwarf spins up, and propeller states (as observed) in which it spins down. We comment on the likely consequences for other magnetic systems.

Key words: accretion, accretion discs – binaries: close – stars: individual: AE Aqr – stars: magnetic fields – novae, cataclysmic variables.

1 INTRODUCTION

AE Aquarii is a cataclysmic variable (CV) system with a white dwarf primary and a K4–K5 type secondary in a 9.88-h orbit, amongst the longest known for a CV. The secondary star is believed to fill its Roche lobe and transfer mass to the white dwarf. AE Aqr is usually placed among the intermediate polar (IP) subclass of CVs, in which the white dwarf is thought to possess a magnetic field in the range $10^4 \lesssim B_* \lesssim 10^7$ G, sufficient to affect significantly the motion of the plasma flow from the secondary, but insufficient to lock the white dwarf into synchronous rotation with the binary orbit. The form of the large-scale accretion flow in IPs is still a matter of vigorous debate. It is known that the magnetic field controls the gas flow close to the surface of the white dwarf, channelling the matter on to restricted regions near the magnetic poles. In consequence, X-rays are produced from shocked gas, which reaches temperatures of $\sim 10^8$ K, near the photosphere of the white dwarf. This emission exhibits modulation at the white dwarf spin period ($P_{\rm spin}$) because of the varying aspect of the accreting poles as a function of spin phase. AE Aqr is observed to be an X-ray source with a luminosity of $L_{\rm X} \sim 5 \times 10^{30}$ erg s^{-1} (Eracleous, Halpern & Patterson 1991), the X-ray flux being modulated at a period of 33.08 s (Patterson et al. 1980; Eracleous, Patterson & Halpern 1991). Eracleous et al. (1994) place the 33-s modulated UV emission (with $L_{\rm UV} \sim L_{\rm X}$) on the white dwarf itself, positively identifying the 33.08-s periodicity as $P_{\rm spin}$, making it the most rapidly spinning white dwarf known. These X-ray and UV luminosity estimates imply an accretion rate of $\dot{M} \lesssim 10^{14}$ g s^{-1} if interpreted as accretion luminosity, much lower than expected from a 10-h binary ($\gtrsim 10^{17}$ g s^{-1}). The rapid spin requires the magnetic field to be low if any matter is to accrete rather than being flung out centrifugally. The corotation radius $R_{\rm co} = (GM_1P_{\rm spin}^2/4\pi^2)^{1/3}$, where field lines move with the local Kepler speed, is only 10^9 cm in AE Aqr, so that material accreted by the white dwarf would have to be threaded by the field close to its surface.

Conventional wisdom is that in low-field, wide-separation systems like AE Aqr, the white dwarf accretes mass from the secondary via a truncated accretion disc (e.g. Patterson

★E-mail: gwy@star.le.ac.uk

1979), material in the inner part of the disc being threaded by the magnetic field and flowing along the field lines. Arguments leading to this conclusion are straightforward: a disc forms in a binary if the accretion flow can initially orbit freely about the primary star (see Frank, King & Raine 1992 for a review). In non-magnetic systems this simply requires the minimum approach distance of the free stream to the primary ($R_{\rm min}$) to exceed the primary star radius (R_1). The situation is more complex if the primary has a significant magnetic field, as this presents a barrier to the accretion stream. In many treatments of IPs it is assumed that the plasma stream can orbit freely about the white dwarf anywhere outside the point where the ram pressure of the stream is of the same order as the magnetic pressure, i.e., $\rho v^2 \sim B^2/8\pi$, where ρ is the stream density, v is the stream velocity, and B is the local magnetic field strength. This condition determines a magnetospheric radius $R_{\rm mag}$, inside which matter is assumed to flow along the magnetic field. The criterion for disc formation in these treatments is then $R_{\rm min} > R_{\rm mag}$. The radius $R_{\rm mag}$ is a difficult quantity to estimate in general, but is usually written as a fraction of the spherical Alfvén radius (e.g. Frank et al. 1992) so that $R_{\rm mag} \propto \mu^{4/7}\dot{M}^{-2/7}$, where μ is the magnetic moment of the white dwarf, and $\dot{M}$ is the accretion rate. For AE Aqr, typical estimates ($M_1 = 0.9\,{\rm M}_\odot$, $\dot{M} = 10^{17}$ g s^{-1}, $\mu = 10^{32}$ G cm^3) give $R_{\rm mag} \sim 10^9$ cm, whereas $R_{\rm min} \gtrsim 10^{10}$ cm, allowing ample room for a disc to form.

Disc accretion should spin up the white dwarf as it acquires the Kepler angular momentum of material at the inner edge. An equilibrium spin period [$P_{\rm eq}$(disc)] is reached at which the white dwarf centrifugally expels as much angular momentum as it accretes. This equilibrium spin period depends on the complex global interaction between the field and the disc, and as yet there is currently no consensus about this. However, it is natural to assume (e.g. Ghosh & Lamb 1979) that this equilibrium occurs when the corotation radius is of order $R_{\rm mag}$. This gives $P_{\rm eq}({\rm disc}) \propto R_{\rm mag}^{3/2} \propto \mu^{6/7}\dot{M}^{-3/7}$, and leads to an equilibrium with $P_{\rm eq}({\rm disc}) \ll P_{\rm orb}$, where $P_{\rm orb}$ is the orbital period of the binary. The rapid white dwarf spin observed in AE Aqr suggests it must have accreted from a disc at some earlier epoch. However, it is unlikely to be doing this currently: the Doppler tomogram of the broad single-peaked Balmer emission lines produced by Horne, Welsh and collaborators (Fig. 1) differs significantly from that expected of an extended accretion disc (cf. Marsh et al. 1990 for U Gem), there being no evidence for an azimuthally symmetric disc flow. We shall see that the unusual properties of AE Aqr can be understood if the white dwarf's rapidly spinning magnetosphere centrifugally ejects most of the transferred mass. The possibility of such flows in IPs was already mentioned by Wynn & King (1995), and we shall follow the treatment of that paper.

Moreover, AE Aqr shows aperiodic variability at several wavelengths, with large-amplitude flares observed in the optical (e.g. Patterson 1979; van Paradijs, Kraakman & Amerongen 1989), radio (Abada-Simon et al. 1995), UV (Eracleous et al. 1994; Eracleous & Horne 1996) and X-ray (Osborne et al. 1995). Flaring behaviour at different wavelengths is not necessarily correlated, and the flaring mech-

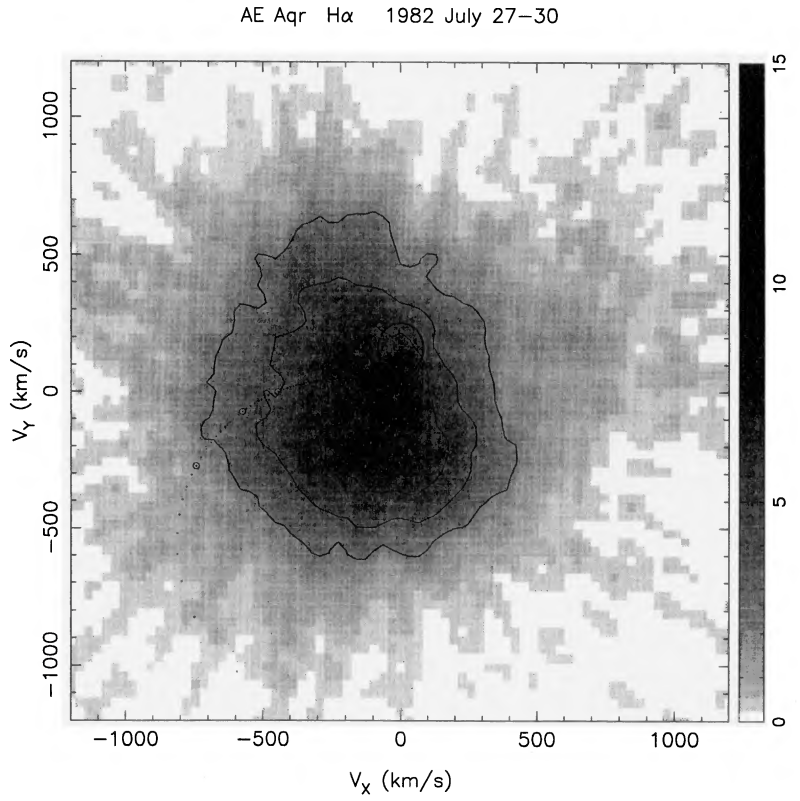

Figure 1. Observed Hα tomogram for AE Aqr. v_x and v_y are inertial velocities plotted with respect to a corotating coordinate system, where the x-axis is along the line of centres of the binary, and the y-axis is in the direction of the instantaneous orbital motion.

anism is not yet understood, but is unique among CVs. The optical flares last between ~ 10 min and 1 h, and have an amplitude up to several magnitudes, making them much larger than the characteristic flickering seen in all CVs, but smaller than dwarf nova eruptions. Quasi-periodic oscillations (QPOs) at periods just longer than $P_{\rm spin}$ are observed during flares (Patterson 1979). AE Aqr is also unique among CVs in being a source of TeV γ-rays (Bowden et al. 1992; Meintjes et al. 1992, 1994), where oscillations have been observed close to $P_{\rm spin}$ with a luminosity of $\sim 2\times 10^{32}$ erg s^{-1}. Furthermore, de Jager et al. (1994) discovered that the white dwarf is spinning down at a rate $\dot{P}_{\rm spin}=5.64\times 10^{-14}$ s s^{-1}, implying a spin-down power $L_{\rm spin}=-I\omega\dot{\omega}\simeq 6\times 10^{33}$ erg s^{-1}, where $I(\sim 10^{50}$ g cm$^2)$ is the white dwarf moment of inertia and $\omega=2\pi/P_{\rm spin}$. This spin-down power exceeds the X-ray and UV luminosities by a factor $\gtrsim 100$, raising the question of the nature of the spin-down torque, which is much greater than any inferred accretion torque.

2 DIAMAGNETIC ACCRETION

King (1993) and Wynn & King (1995) modelled the mass flow in IPs as a set of large, diamagnetic gas blobs. There is considerable observational evidence for a highly inhomogeneous accretion stream in the AM Her stars (e.g. Hameury & King 1988; Watson et al. 1989; Beardmore & Osborne 1996), and theory provides several reasons to believe that the gas flow in IPs may also be broken up into such blobs, either at the L_1 point (King 1989) or by the plethora of magnetohydrodynamic instabilities operating as the gas stream encounters the magnetosphere (e.g. Elsner & Lamb 1977; Arons & Lea 1980; Aly & Kuijpers 1990). In this paper we shall assume that blobs are formed close to the L_1 point, although the results presented in the following sections should apply to any situation in which blobs are formed in the outer reaches of the primary's Roche lobe.

In such an inhomogeneous flow, blobs penetrate the magnetosphere rather than being forced into a field-aligned flow (King 1993). As the blobs move through the magnetosphere they interact with the local field B via a surface drag term (Drell, Foley & Ruderman 1965), exchanging orbital energy and angular momentum with the white dwarf. Blobs of density $\rho_{\rm b}$ and length $l_{\rm b}$ lose energy on a time-scale.

$$t_{\rm mag}\simeq\frac{c_{\rm A}\rho_{\rm b}l_{\rm b}}{B^2}\frac{|\boldsymbol{v}_\perp|}{|[\boldsymbol{v}-\boldsymbol{v}_{\rm f}]_\perp|}, \qquad (1)$$

where $c_{\rm A}$ is the Alfvén speed in the interblob plasma, $\boldsymbol{v}$ and $\boldsymbol{v}_{\rm f}$ are the blob and field velocities, and the suffix $\perp$ denotes the velocity components perpendicular to the field lines. Typical estimates give the hierarchy of time-scales $t_{\rm dyn}<t_{\rm mag}<t_{\rm visc}$, where $t_{\rm dyn}=(r^3/GM_1)^{1/2}$ is the dynamical time-scale of the blobs, and $t_{\rm visc}$ is the viscous time-scale on which an accretion disc can form by self-interaction. For slow rotators ($|\boldsymbol{v}_{\rm f}|\ll|\boldsymbol{v}|$) this time-scale reduces to $t_{\rm mag}({\rm slow})\sim c_{\rm A}\rho_{\rm b}l_{\rm b}/B^2$. Accordingly the blobs follow ballistic trajectories modified by the magnetic acceleration

$$\boldsymbol{g}_{\rm mag}=-k[\boldsymbol{v}-\boldsymbol{v}_{\rm f}]_\perp, \qquad (2)$$

where $k\sim 1/t_{\rm mag}({\rm slow})$ is the drag coefficient. An important consequence of this simple prescription is that the velocity difference introduces the quantity $P_{\rm spin}$ into $\boldsymbol{g}_{\rm mag}$, so that $P_{\rm spin}$ now directly influences the magnetospheric gas flow. This is in direct contrast to the pressure balance argument outlined in the previous section, which is insensitive to $P_{\rm spin}$.

Blob orbits and the spin evolution of the white dwarf were examined by King (1993) and Wynn & King (1995) both analytically and numerically. A major result is that blobs may be either accreted or ejected, depending on $P_{\rm spin}$ and k. This dictates a spin equilibrium for the white dwarf with $P_{\rm spin}\propto P_{\rm orb}$, the coefficient of proportionality being about 0.07. Once the white dwarf has attained spin equilibrium (in a time $t_{\rm spin}\sim 10^5$ yr), the mass flow pattern can be computed using a particle code developed by Whitehurst (1988). The predicted emission-line profiles and Doppler tomogram of the equilibrium flow pattern then provides a direct observational test of the model. Wynn & King (1995) pointed out that stable cases were possible in which the white dwarf ejects almost all of the matter transferred to it.

In order to simulate the gas flow in AE Aqr, we adopt the simple prescription of Wynn & King (1995) in which $k\sim B^2/c_{\rm A}\rho_{\rm b}l_{\rm b}\sim k_0(r/r_0)^{-n}$, where k_0, n and r_0 are constants. To estimate k_0 we require estimates of the rather uncertain parameters of the dense plasma blobs. At a radius $r=10^{10}$ cm from the white dwarf the accretion stream has a typical density $\rho_{\rm b}\sim 10^{-9}P_{\rm h}^{-2}\sim 10^{-11}$ g cm^{-3}, where $P_{\rm h}$ is the orbital period in hours (e.g. Frank, King & Lasota 1988). A shot-noise analysis of AM Her leads to an estimate $l_{\rm b}\sim 10^9$ cm at a similar distance from the white dwarf (Beardmore & Osborne 1996). Parametrizing $\rho_{\rm b}$, $l_{\rm b}$ in terms of these estimates and assuming spherical blobs, we have

$$k_0\sim 3\times 10^{-9}B(r_0)^2\rho_{-11}^{-1}l_9^{-1}\quad {\rm s}^{-1}, \qquad (3)$$

with $r_0=10^{10}$ cm, where ρ_{-11} is $\rho_{\rm b}$ in units of 10^{-11} g cm^{-3}, and l_9 is the blob length in units of 10^9 cm. Here we have implicitly assumed that the density in the tenuous plasma surrounding the blobs is $<10^{-11}$ g cm^{-3}, in which regime $c_{\rm A}$ is equal to the speed of light. Following Wynn & King (1995, section 2) this leads to $k\propto r^{-2}$, which, together with equation (3), defines the drag coefficient for the purposes of the simulations. For comparison, we also consider the case in which $k\propto r^{-3}$, suggested by King (1993) and examined in Wynn & King (1995).

A further consideration arises when considering the dynamics of such an inhomogeneous gas flow in AE Aqr: because of the rapid spin rate of the white dwarf, the light cylinder (defined by the radius, $R_{\rm L}$, at which the velocity of the magnetic field lines approaches the speed of light) lies close (at 1.6×10^{11} cm) to the binary separation, a (1.8×10^{11} cm). Outside $R_{\rm L}$ the field must be wound up, and it falls off as r^{-1}. Magnetic effects are unimportant here, and in particular no further acceleration of the blobs is possible.

3 DYNAMICS OF THE GAS FLOW IN AE AQR

In order to simulate the gas flow in AE Aqr, we use the following fixed parameters: $P_{\rm orb}=9.9$ h, $P_{\rm spin}=33$ s, $M_1=0.9\,{\rm M}_\odot$ (de Jager et al. 1994) and $q=0.64$ (Eracleous et al. 1994). We assume $P_{\rm spin}=33$ s at the onset of mass transfer, and comment later on this assumption. An arbitrary random variation in the magnetic of k_0 about the value given by equation (3) is implemented for each blob to simulate a

distribution of blob densities and length-scales. The variation is of the form of a uniform distribution with limits $k_0 \pm \eta k_0$, where η was varied between 0.2 and 0.7. This random variation has little effect on the results, and the discussion below is general.

A typical flow pattern obtained from the above parameters is shown in Fig. 2. As can be seen, most ($\gtrsim$99 per cent) of the mass transferred is ejected from the system via a gas stream in the plane of the binary. The ejection of gas from the system requires rapid rotation of the white dwarf, which gives rise to a large relative velocity between the plasma blobs and the B-field in the plane of the binary. The blobs gain orbital energy and angular momentum as they pass through the magnetosphere, spinning down the white dwarf, and cruise out of the system to form a disc of material extending out to large radii.

The exact trajectory of the stream is dependent on k alone, since we have assumed $P_{\rm spin}$ to be fixed. We have also implicitly assumed that $\dot{M}$ does not affect the trajectory of the blobs, i.e., that a change in the mass transfer rate does not significantly alter the blob parameters ($\rho_{\rm b}$ and $l_{\rm b}$), and hence k_0. We can then adjust k, through k_0 and n, in order to obtain agreement between the observed Doppler tomogram and that predicted by the simulated gas flow. A typical flow pattern is that of Fig. 2, and its tomogram is shown in Fig. 3. Blobs reach a maximum velocity of $v_{\rm esc} \lesssim 1000$ km s^{-1} at closest approach to the white dwarf ($\gtrsim 10^{10}$ cm), and cruise out of the system with a velocity of $v_\infty \simeq 300$ km s^{-1}.

The calculated Doppler tomogram for the magnetic propeller model (Fig. 3) may be compared with the observed tomogram (Fig. 1). The agreement is clearly not perfect, but there are important similarities. In both observed and computed tomograms, the emission is primarily in the lower-left quadrant (V_X, V_Y both negative). In the computed tomogram, the two regions most densely populated by blobs are located near the inner Lagrangian point, where the blob velocities are still low, and where the blobs are decelerating as they leave the binary system (V_X small, V_Y negative and decreasing toward zero). A relatively low blob density is present in the region of closest approach (the 'loop' at high velocities in the lower-left quadrant), because the velocity vector is rapidly changing as the blobs move quickly through this part of the map.

The observed tomogram has a broad asymmetric peak centred at relatively low velocities in the lower-left quadrant of the map. It is normally very difficult to account for a tomogram of this form, because there is no obvious part of the binary system that moves with this velocity vector. However, the observed tomogram does resemble a rather highly blurred version of the computed tomogram for the magnetic propeller. In particular, the emission regions at the L_1 point and along the $-V_Y$ axis can just be distinguished. While there is no clear evidence for the 'loop', this may be lost in the high degree of Doppler blurring, which produces emission at velocities of order 700–1000 km s^{-1} in the upper-left, upper-right and lower-right quadrants, where

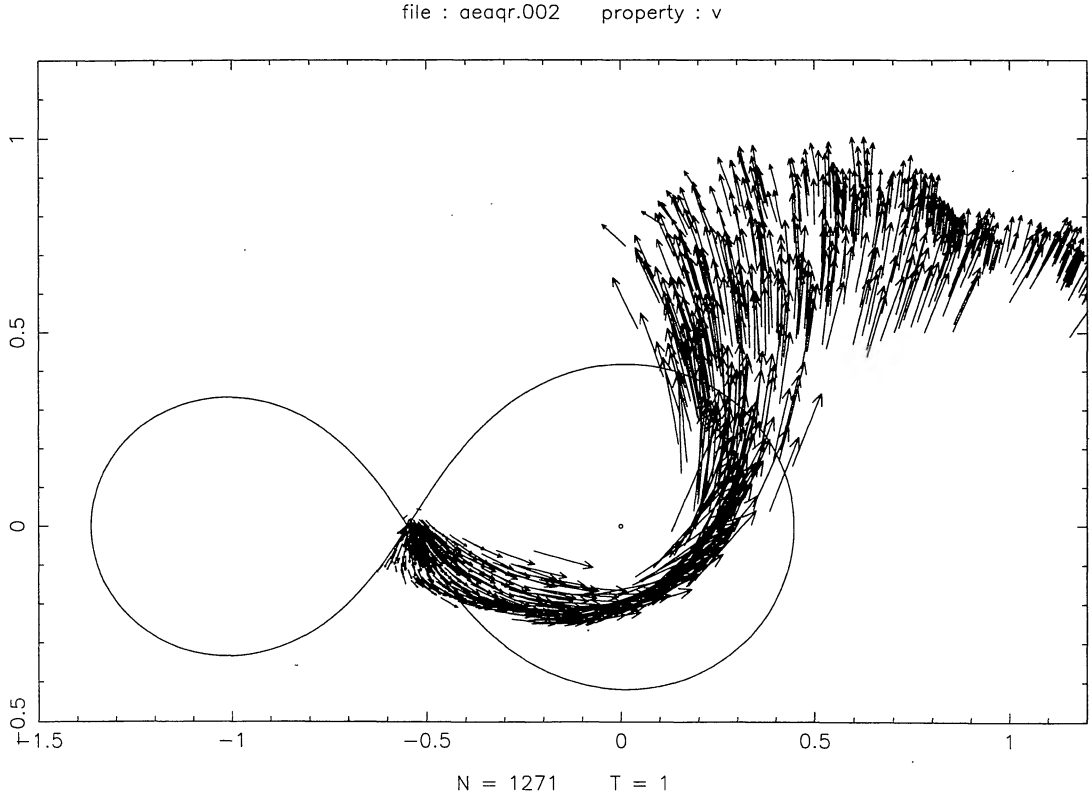

Figure 2. Simulated inhomogeneous, diamagnetic gas flow in AE Aqr. The figure shows the Roche lobes of the primary and secondary, the orbital motion being in a clockwise direction. Inertial frame velocity vectors (arbitrary units) are plotted for each particle. Note that the (x, y) coordinate system is the reverse of that indicated in the Doppler tomograms (Figs 1 and 3).

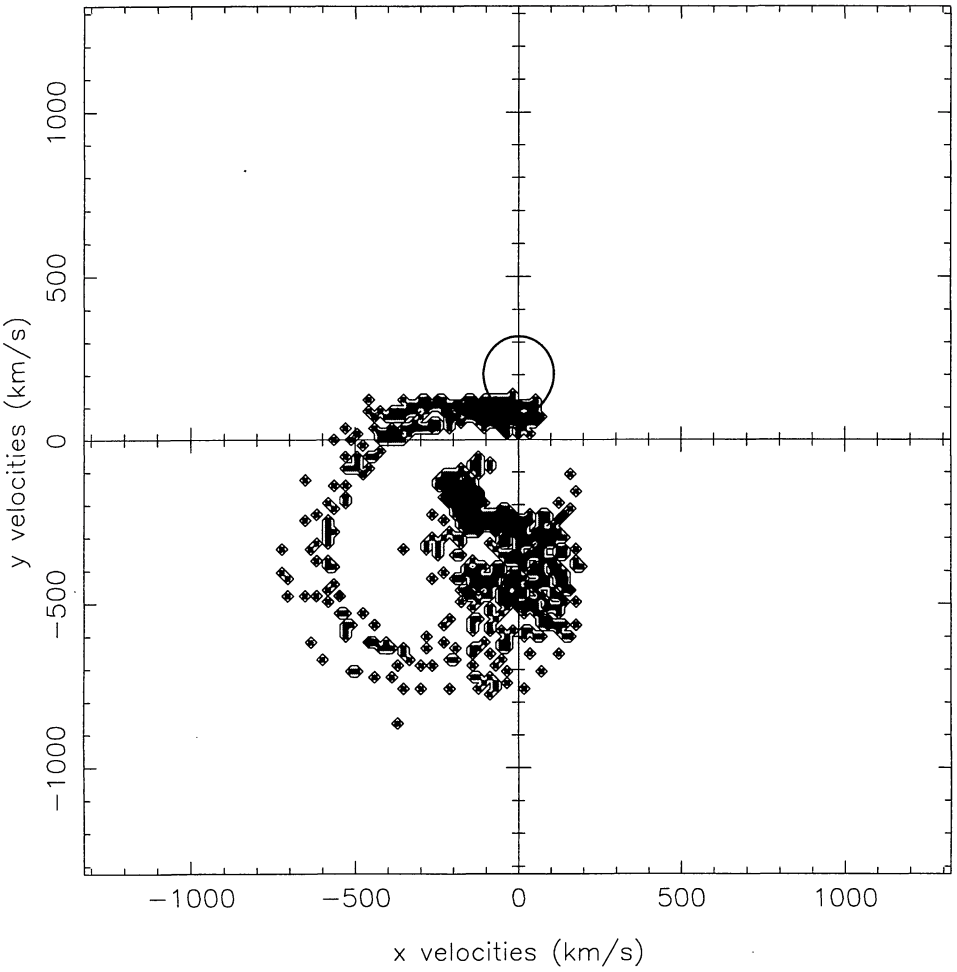

Figure 3. Simulated Doppler tomogram of the gas flow of Fig. 2. The tomogram was produced assuming a system inclination of 55°.

the magnetic propeller predicts hardly any emission. We conclude that the magnetic propeller model has some success in accounting for the general features of the observed tomogram, but we still require some additional source of Doppler blurring to account for the broad wings.

Note that to account for the observed tomogram in more detail, we should really weight each blob by the changing intensity of the Hα emission it emits at each point along its path through the tomogram. In Fig. 3 we have assumed that the blobs emit Hα at a constant rate, then cut off suddenly when they reach a particular radius.

For clarity, the orbit of a single particle and the trajectory through tomogram velocity space are presented in Figs 4 and 5, for three values of k_0. The origin of the computed tomogram can be seen from the figures for the case in which $k_0 = 10^{-5}$ s^{-1}.

The particle orbits are very sensitive to the drag coefficient k_0 as shown in Figs 4 and 5, and the observed tomogram places tight constraints on its magnitude. If k is too low the blobs are able to make at least one full orbit about the white dwarf, producing a ring-like structure on the simulated tomogram, whereas if k is too high the blobs are ejected with positive rather than negative y-velocities. Our estimates place k_0 in the range $(1\text{–}5) \times 10^{-5}$ s^{-1}. These constraints on k_0, from equation (3), lead to limits on the white dwarf magnetic moment $\mu = B(r)r^3$. We find

$$\mu \simeq 1.8 \times 10^4 (k_0 \rho_{-11} l_9)^{1/2} r_0^3 \sim 10^{32} (l_9 \rho_{-11})^{1/2} \quad \text{G cm}^3, \qquad (4)$$

consistent with the expected range of magnetic moments for IPs. Given k_0, it is also possible to determine the mass transfer rate, $\dot{M}$, to account for the observed $L_{\rm spin}$. Given the observed system parameters, the spin-down power is a function of k and $\dot{M}$ only, with $L_{\rm spin}\omega^{-1} \sim \dot{M}(r_{\rm esc} v_{\rm esc} - b^2\Omega)$, where $r_{\rm esc}$ and $v_{\rm esc}$ are determined by k_0, and $b^2\Omega$ is the specific angular momentum of blobs leaving L_1 (where b is the distance of the L_1 point from the centre of the primary, and $\Omega = 2\pi/P_{\rm orb}$). Numerical experiments which evolve the spin rate of the white dwarf, similar to Wynn & King (1995), confirm that $L_{\rm spin}$ scales linearly with $\dot{M}$, and give a mass overflow rate of

$$10^{17} \lesssim \dot{M} \lesssim 5 \times 10^{17} \text{ g s}^{-1}, \qquad (5)$$

for $L_{\rm spin} = 6 \times 10^{33}$ erg s^{-1}. These predicted mass transfer rates are close to those deduced for nova-like variables at similar orbital periods (e.g. Dhillon 1996). Furthermore, the estimate is consistent with the estimated $\dot{M} \sim 4 \times 10^{17}$ g s^{-1} required to power the UV emission lines observed in the system (Eracleous & Horne 1996).

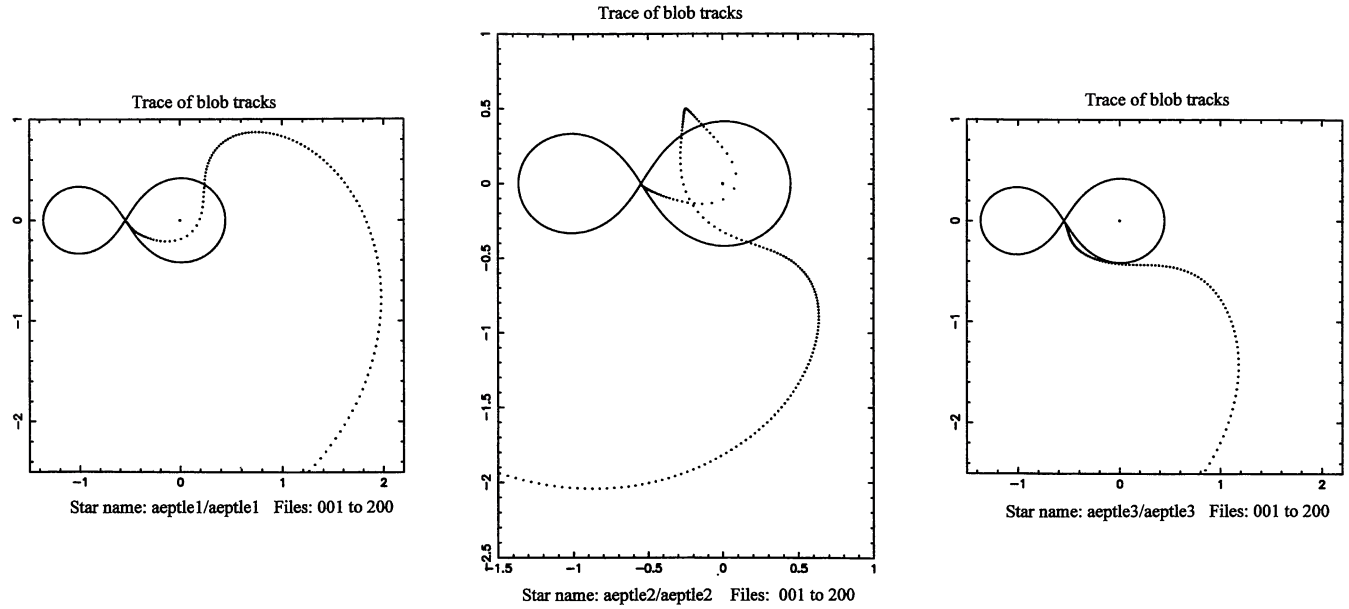

Figure 4. Single-particle orbits for various values of k_0 and $k \propto r^{-2}$, shown in a frame corotating with the binary. The left-hand panel shows the orbit for $k_0 = 10^{-5}$ s^{-1}, the centre panel is for $k_0 = 5 \times 10^{-6}$ s^{-1}, and the right-hand panel is for $k_0 = 5 \times 10^{-5}$ s^{-1}.

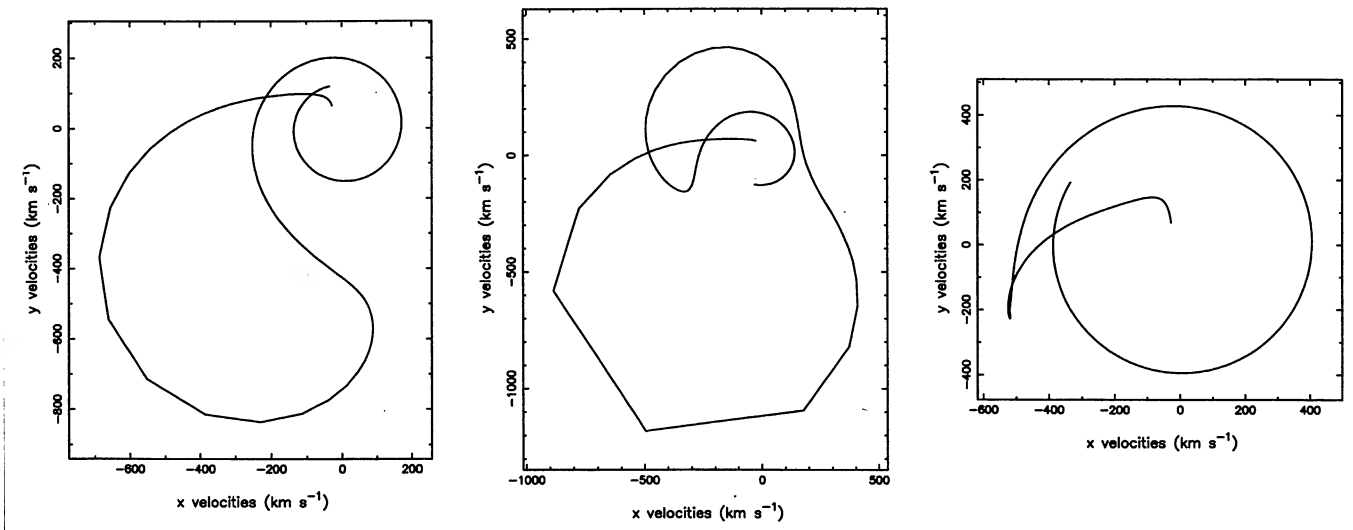

Figure 5. Velocity-space trajectories of the orbits shown in Fig. 4. The plots show the true values of the inertial velocities (i.e., an inclination of 90°).

The estimates above apply to the $k \propto r^{-2}$ model for the diamagnetic drag force. The $k \propto r^{-3}$ model gives very similar values for μ and $\dot{M}$, but the white dwarf magnetic moment is less well constrained, with $\mu \sim (10^{31}$–$10^{33})\,(l_9 \rho_{-11})^{1/2}$ G cm^3.

Estimate (5) gives the rotational energy loss rate of the white dwarf in expelling blobs as $L_{\rm esc} \sim \dot{M} v_{\rm esc}^2/2 \sim$ few $\times\, 10^{33}$ erg s^{-1}, where the escape velocity $v_{\rm esc} \sim 1000$ km s^{-1}. Hence a significant fraction of the spin-down power goes into supplying the mechanical energy of the ejecta, $L_{\rm spin} \sim L_{\rm esc}$, explaining the discrepancy between the spin-down power and the observed radiative luminosity. However, the interaction between the plasma blobs and the B-field is a dissipative process (cf. King 1993). Since k and $\dot{M}$ have been fixed independently, the model gives an estimate of the local magnetic dissipation rate $L_{\rm mag} = -k[\boldsymbol{v} - \boldsymbol{v}_{\rm f}]_\perp^2$ as

$$L_{\rm mag} \sim 10^{33} \text{ erg s}^{-1}. \quad (6)$$

We speculate on the form of this dissipation in Section 6. However, assuming that some fraction of $L_{\rm mag}$ appears as emission lines, it is possible to weight the simulated tomogram with the predicted dissipation rate. The dissipation rate for a single particle in the $k \propto r^{-2}$ and $k \propto r^{-3}$ models is shown in Fig. 6. We see that the dissipation rate in the $k \propto r^{-2}$ case is almost constant (within a few per cent), and hence has a negligible effect on the tomogram. However, the $k \propto r^{-3}$ case shows a steep rise by a factor $\simeq 4$ near

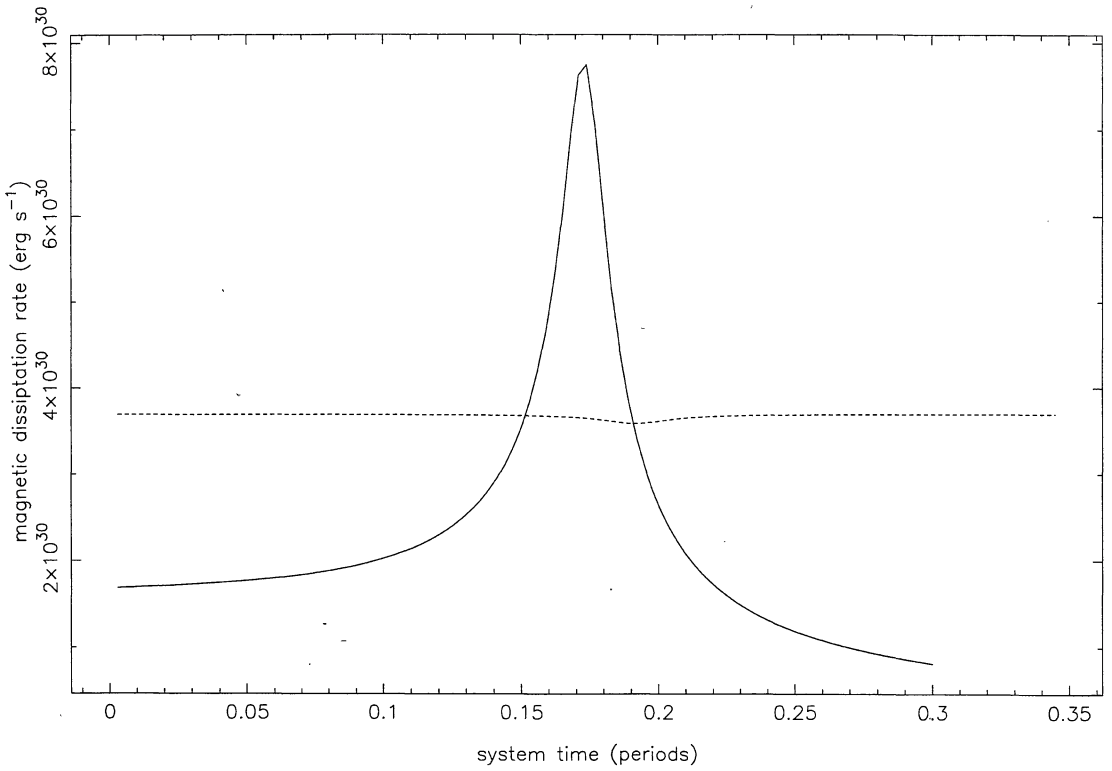

Figure 6. Local dissipation rate $L_{\rm mag}$ for a single particle released from L_1 at time 0 in the cases $k \propto r^{-2}$ (dashed line) $k \propto r^{-3}$ (full line). The trough of the dashed curve and the peak of the full curve correspond to the particle's closest approach to the white dwarf.

closest approach of the particle to the white dwarf. This increases the emission of particles near closest approach, producing a noisy tomogram, which can be dominated by 'flares' from the stream close to the white dwarf. We comment on this alternative in the discussion.

To check our results we performed three-dimensional simulations of the inhomogeneous, diamagnetic gas flow in AE Aqr. In these models a full dipole field structure is employed, and a typical flow pattern is shown in Fig. 7. The general results do not differ from those outlined above, as the ejecta remain close to the orbital plane, and the rotation of the magnetosphere is rapid enough to average out any azimuthal variation of the field strength. From Fig. 7 it is possible to estimate the opening angle of the stream as $\sim 10°$.

4 THE FATE OF THE EXPELLED BLOBS

The results of the previous section were obtained by assuming that the blobs remained intact during the interaction with the magnetosphere of the white dwarf. This assumption is not necessarily correct. Plasma instabilities, such as the Kelvin–Helmholtz instability, resulting from the large shear between the blobs and the external magnetic field (e.g. Arons & Lea 1980), as well as the differential nature of the drag force itself, act to disrupt the blobs. The agreement between the observed tomogram of Fig. 1 and that predicted in Fig. 3 suggests that the blobs remain intact until they pass closest approach and are ejected. Near closest approach the strong shear between the blobs and the field, as well as the effect of the drag force, may tear the blobs apart. The fine droplets of low-density plasma which should result from such an event would be quickly threaded by the magnetic field, spun up and ejected, as threading would occur well outside corotation. The azimuthal velocity of the field at closest approach ($\sim 10^{10}$ cm) is $\sim 10^4$ km s^{-1}. Since such a high-velocity component is not observed, we may assume that either the blobs survive the encounter intact, or the resulting plasma is somehow ejected at velocities much lower than the local field velocity.

Once ejected, the blobs cruise out of the system to large radii. The spiral path of the ejecta is shown in Fig. 8. The velocity dispersion within the ejecta $\Delta v/v \sim 1/10$ implies that the density peaks diffuse and the spirals merge at a distance $r \sim 10a$. Eracleous & Horne (1996) estimate the density of the line-emitting gas of the ejecta as it leaves the Roche lobe of the white dwarf to be $\sim 10^{-16}$ g cm^{-3}, using the presence of semiforbidden lines. If the blobs remain intact during their passage through the magnetosphere of the white dwarf, they should expand at the sound speed of the blob gas as they leave the system. Any such expansion (blob sound speed ~ 10 km s^{-1}) would be insufficient to allow the blobs to reach the densities predicted by the emission-line observations, for reasonable blob parameters. For the blobs to reach the observed low densities would require expansion at a velocity of ~ 100 km s$^{-1} \sim v_{\rm esc}$. Such a high velocity is clearly too large for any reasonable blob sound speed, and would suggest that the blobs were disrupted in the magnetosphere if associated with the line emission. However, the

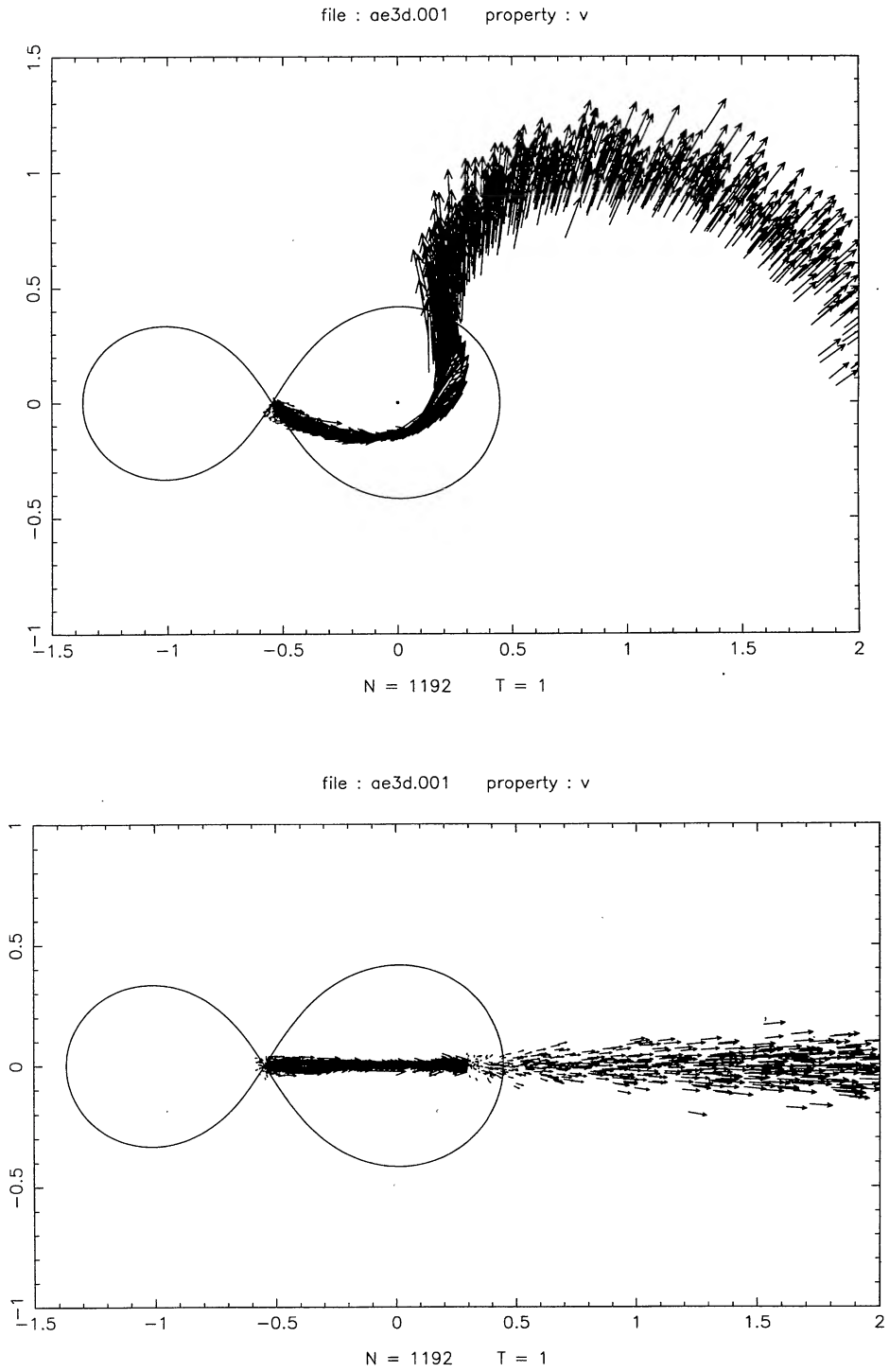

Figure 7. 3D simulation of inhomogeneous, diamagnetic gas flow in AE Aqr. The upper panel shows the system at the same orientation as the 2D simulation of Fig. 2. The lower panel shows the system viewed in the orbital plane. In this simulation the magnetic dipole of the white dwarf was inclined at an angle of 60° to its spin axis.

simulations presented in the previous section only take account of the mass flow in the form of dense gas blobs. Any low-density component of the mass flow is neglected in the simulations. Since the observations sample only the line-emitting regions of the gas flow, it may be that this arises from a low-density component present throughout the flow, perhaps progressively stripped from the blobs.

5 A POSSIBLE ACCRETION HISTORY FOR AE AQR

We have seen above that the diamagnetic blob picture gives a consistent framework for understanding the observed features of AE Aqr. We now consider the spin evolution of the system.

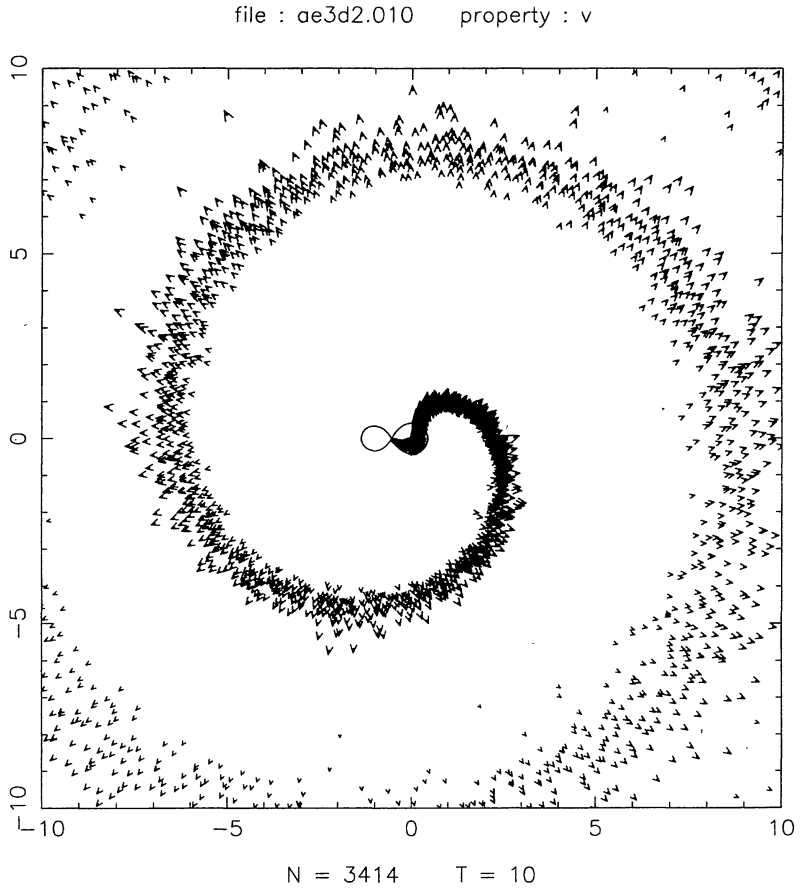

Figure 8. Large-scale view of the ejected mass in the simulated inhomogeneous gas flow in AE Aqr.

At the onset of mass transfer we assume AE Aqr to have an initial orbital period $\gtrsim 10$ h, and a μ and $\dot{M}$ in line with the estimates (4) and (5). For diamagnetic blob accretion we must take into account the spin of the white dwarf. It is probable that the initial spin period of the white dwarf was much longer than the current value of 33 s; if we assume $P_{\rm spin} \gtrsim 1$ h initially, the velocity difference in (2) at $r \sim R_{\rm min} \sim 10^{10}$ cm allows blobs to orbit freely about the white dwarf. Since $t_{\rm visc} < t_{\rm mag}$, we would expect the build-up of mass around the white dwarf to cause the blobs to merge and eventually initiate the formation of an accretion disc. This assumption is confirmed by numerical experiment for $P_{\rm spin} \gtrsim 1$ h (cf. Fig. 9).

Once an accretion disc has formed, the white dwarf will spin up to the rapid equilibrium spin period $P_{\rm eq}$(disc), as outlined in Section 1. With $P_{\rm eq}$(disc) ~ Kepler period at $R_{\rm mag}$, we have

$$P_{\rm eq}({\rm disc}) \sim 50\, m_1^{-5/7} \dot{M}_{17}^{-3.7} \mu_{32}^{6/7}\ {\rm s}, \qquad (7)$$

where m_1 is the mass of the white dwarf in solar masses, $\dot{M}_{17}$ is $\dot{M}$ in units of 10^{17} g s^{-1}, and μ_{32} is μ in units of 10^{32} G cm^3. Thus a spin period $\lesssim 30$ s implies $\mu_{32} \lesssim 1$, agreeing well with our previous estimate (4).

Once the white dwarf has been spun up, it will remain stable at $P_{\rm eq}$(disc) as long as the disc remains approximately steady. We deduce that $\dot{M}$ must have varied in AE Aqr in the past, at least on short time-scales. If $\dot{M}$ drops to a value low enough to allow the accretion disc to be eroded (in at time ~ weeks typically), then even when the mass transfer rate returns to its previous value, the flow must now interact with a rapidly rotating magnetosphere ($P_{\rm spin} \sim 30$ s). The numerical calculations of the diamagnetic gas flow in Section 3 were initiated with $P_{\rm spin} = 33$ s, in order to simulate the plasma–magnetosphere interaction after just such a low phase of mass transfer. Compared to the initial disc formation phase with $P_{\rm spin} \gtrsim 1$ h, $g_{\rm mag}$ has increased by two or three orders of magnitude because of the increased value of the velocity difference in (2), corresponding to $P_{\rm spin} \sim 30$ s. Hence blobs gain angular momentum and are rapidly expelled from the system as they approach $R_{\rm min}$, as shown in Section 3.

By contrast, in the homogeneous stream treatment outlined in Section 1 AE Aqr is always an ideal system for an accretion disc to form, having long $P_{\rm orb}$ (and thus large $R_{\rm min}$) and a relatively low magnetic moment. Such a system could never become a propeller, contrary to observation, as the disc formation criterion is independent of $P_{\rm spin}$. Henceforth we consider only the blob model.

Once in the propeller state, we need to consider the dynamical stability of the mass transfer process since orbital angular momentum is carried away with the ejecta. This process in principle could cause the Roche lobe to close in on the secondary star, ultimately resulting in runaway mass transfer. The situation was considered in Wynn & King (1995), where the condition for stability was found as

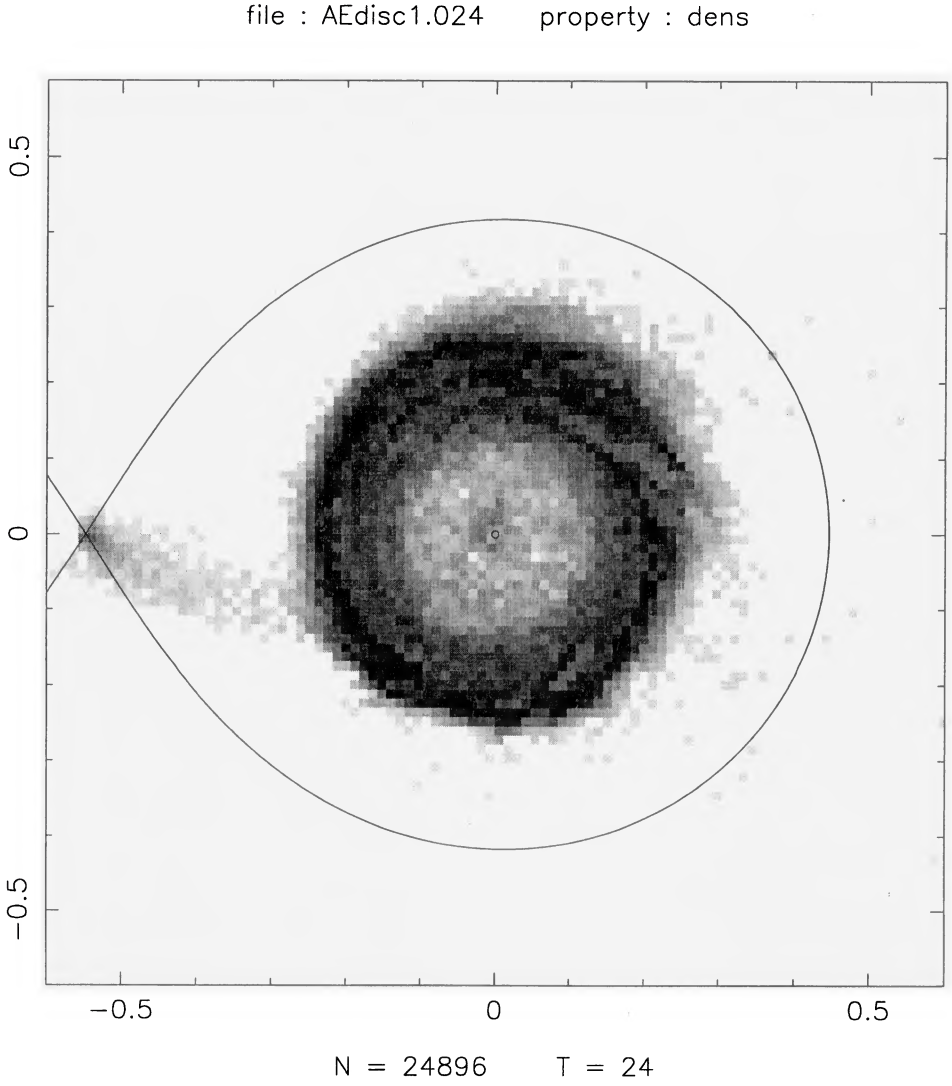

Figure 9. Simulation of the gas flow in AE Aqr using the magnetic drag prescription, and setting $P_{\rm spin}=1$ h.

$$\frac{5}{6}+\frac{\zeta_{\rm ad}}{2}-(1-\alpha)q-\frac{1}{3}\frac{q\alpha}{(1+q)}-\eta(1+q)\left(\frac{b}{a}\right)^2>0, \qquad (8)$$

where q is the mass ratio M_2/M_1, α is the fraction of transferred mass lost from the system, η is the fraction of orbital angular momentum possessed by the transferred mass which is lost from the binary, and $b/a=0.5$–$0.227\log q$. The adiabatic index of the secondary star's envelope ($\zeta_{\rm ad}$) is given by

$$\frac{\dot{R}_2}{R_2}=\zeta_{\rm ad}\frac{\dot{M}_2}{M_2}, \qquad (9)$$

where R_2, M_2 are the mass and radius of the secondary respectively. The secondary star in AE Aqr has a mass $\sim 0.6\,{\rm M}_\odot$ and fills its Roche lobe in a 10-h binary, making it much larger than its main-sequence radius. The star must have been somewhat nuclear-evolved before angular momentum losses brought about contact. Hjellming & Webbink (1987) find $\zeta_{\rm ad}$ for such a star to lie in the range -0.2 to -0.3. Thus the long-term ($\sim 10^7$ yr) ejection process in AE Aqr is dynamically stable, since $\alpha=\eta=1$ (cf. Wynn & King 1995).

This stability of the mass ejection process introduces the possibility of cyclic behaviour. As the white dwarf is spun down during the ejector phase it will approach the equilibrium spin period $P_{\rm spin}\sim 0.07P_{\rm orb}$ for IPs, as outlined in Section 2 (we note that the equilibrium $P_{\rm spin}\sim 0.07P_{\rm orb}$ is not a general equilibrium for all asynchronous magnetic CVs, but for a subset which accrete via diamagnetic gas blobs). However, this spin period is never reached, as the increase in $P_{\rm spin}$ allows the formation of an accretion disc (Fig. 9), which once again spins up the white dwarf to $P_{\rm spin}\sim 30$ s. The system will again become an ejector if mass transfer ceases for a disc flushing time, so it is likely to cycle between phases of disc accretion and ejection. The duration of the disc phase depends on the short-term stability of mass transfer. The fact that disc accretion is currently observed in DQ Her ($P_{\rm spin}=71$ or 142 s) suggests that this phase can be quite long-lived. It is noticeable that DQ Her appears to have a very steady accretion rate.

6 DISCUSSION

The picture of AE Aqr outlined in this paper differs radically from the usual scenario (e.g. Patterson 1979), which would predict that an accretion disc is always present. Instead, we have a picture in which the system has no disc at all, but expels most of the transferred mass with little or no accretion taking place. The atypical Doppler tomogram of Fig. 1, and the large spin-down torque exerted on the white dwarf are natural consequences of the inhomogeneous diamagnetic accretion model, in which the criterion for disc formation involves the white dwarf spin. The discrepancy between the large spin-down power of the white dwarf and the observed luminosity of the system is explained by the kinetic energy carried away by the ejecta. Constraining the model parameters to agree with observation gives an estimate of the white dwarf magnetic moment and an estimate of the mass transfer rate consistent with that expected for an IP with an orbital period of 10 h. Moreover, the magnetic moment estimate obtained from the diamagnetic blob model agrees well with that required, if we assume that the current short spin period resulted from a previous phase of disc accretion.

The diamagnetic blob model also predicts a magnetic dissipation rate $\sim 10^{33}$ erg s^{-1}. The nature of this magnetic dissipation is uncertain. A small fraction of this energy may be carried down to the white dwarf surface in the form of Alfvén waves excited by the blobs as they plough through the magnetosphere, giving rise to the observed UV and X-ray hotspots. Eracleous & Horne (1996) suggest that shock heating of the blobs as they encounter the magnetosphere may power the observed UV emission lines. If this process is controlled by the magnetic dissipation, then a stable observed tomogram would favour the $k \propto r^{-2}$ model for the drag coefficient, while a highly variable tomogram dominated by flares in the negative x and y velocity quadrant would favour the $k \propto r^{-3}$ model. One attractive feature of the shock-heated blob model is the possibility of explaining the QPOs sometimes observed in the flares: the QPOs would be associated with the relative angular velocity $\omega_r = \omega(\text{field}) - \omega(\text{blob})$ between the blob and the magnetic field. This gives periods very close to $P_{\rm spin}$, except near closest approach where the period is in the range 33.5–34 s, in rough agreement with the observed QPO periods.

These processes could account for only $\lesssim 1$ per cent of $L_{\rm mag}$, however. A significant fraction of this energy may go into particle acceleration and the production of γ-rays (cf. Meintjes & de Jager 1995). The large shear beween the field and the blob stream may induce current instabilities in the interblob plasma, producing double layers which are able to accelerate electrons and protons to energies in excess of 1 TeV. Such high-energy emission may carry off the predicted $L_{\rm mag}$, but this idea requires further detailed consideration (e.g. Kuijpers et al. 1996).

The cyclic behaviour discussed in the previous section may be generic to all IPs. However, if μ is much higher than 10^{32} G cm^3, the system will reach the equilibrium position $P_{\rm spin} \sim 0.07 P_{\rm orb}$ without reforming a disc after the first ejection phase. This equilibrium ($\alpha \sim \eta \sim 0.1$) gives dynamically stable mass transfer only for $q \lesssim 0.7$, so that IPs close to this equilibrium should have $P_{\rm orb} \lesssim 6$ h, as observed (cf. Wynn & King 1995). These systems should have accretion flows which are strongly influenced by the magnetic field throughout. Since $t_{\rm mag} < t_{\rm visc}$, a Keplerian disc could only re-form if the mass transfer rate rose significantly.

ACKNOWLEDGMENTS

We thank Bill Welsh for supplying the tomogram of Fig. 1, and Mike Eracleous for useful discussions.

REFERENCES

Abada-Simon M., Bastian T. S., Horne K., Robinson E. L., Bookbinder J. A., 1995, in Buckley D. A. H., Warner B., eds, ASP Conf. Ser. 85, Cape Workshop on Magnetic Cataclysmic Variables. Astron. Soc. Pac., San Francisco, p. 355
Aly J. J., Kuijpers J., 1990, A&A, 227, 473
Arons J., Lea S. M., 1980, ApJ, 235, 1016
Beardmore A. P., Osborne J. P., 1996, MNRAS, submitted
de Jager O. C. et al., 1994, MNRAS, 267, 577
Dhillon V., 1996, in Evans A., Wood J. H., eds, Cataclysmic variables and related objects. Kluwer, Dordrecht, p. 3
Drell S. D., Foley H. M., Ruderman M. A., 1965, J. Geophys. Res., 70, 3131
Elsner R. F., Lamb F. K., 1977, ApJ, 215, 897
Eracleous M., Horne K., 1996, ApJ, 471, 427
Eracleous M., Halpern J., Patterson J., 1991, ApJ, 382, 290
Eracleous M., Patterson J., Halpern J., 1991, ApJ, 370, 330
Eracleous M., Horne K., Robinson E. L., Zhang Z., Marsh T. R., Wood J. H., 1994, ApJ, 433, 313
Frank, J., King A. R., Lasota J. P., 1988, A&A, 193, 113
Frank J., King A. R., Raine D. J., 1992, Accretion Power in Astrophysics, 2nd edn. Cambridge Univ. Press, Cambridge
Ghosh P., Lamb F. K., 1979, ApJ, 232, 259
Hameury J. M., King A. R., 1988, MNRAS, 235, 433
Hameury J. M., King A. R., Lasota J. P., 1986, MNRAS, 218, 695
Hjellming M. S., Webbink R. F., 1987, ApJ, 318, 794
King A. R., 1989, MNRAS, 241, 365
King A. R., 1993, MNRAS, 261, 144
Kuijpers J., Abada-Simon M., Fletcher L. D., Horne K., Raadu M. A., Steeghs D., 1996, A&A, submitted
Marsh T. R., Horne K., Schlegel E. M., Honeycutt R. K., Kaitchuk R. H., 1990, ApJ, 364, 637
Meintjes P. J., de Jager O. C., 1995, in Buckley D. A. H., Warner B., eds, ASP Conf. Ser. 85, Cape Workshop on Magnetic Cataclysmic Variables. Astron. Soc. Pac., San Francisco, p. 396
Meintjes P. J., Raubenheimer B. C., de Jager O. C., Brink C., Nel H. I., North A. R., van Urk G., Visser B., 1992, ApJ, 401, 325
Meintjes P. J., de Jager O. C., Raubenheimer B. C., Nel H. I., North A. R., Buckley D. A. H., Koen C., 1994, ApJ, 434, 292
Osborne J. P., Clayton K. L., O'Donoghue D., Eracleous M., Horne K., Kanaan A., 1995, in Buckley D. A. H., Warner B., eds, ASP Conf. Ser. 85, Cape Workshop on Magnetic Cataclysmic Variables. Astron. Soc. Pac., San Francisco, p. 368
Patterson J., 1979, ApJ, 234, 978
Patterson J., Branch D., Chincarini G., Robinson E. L., 1980, ApJ, 240, L133
van Paradijs J., Kraakman H., van Amerongen S., 1989, A&AS, 79, 205
Watson M. G., King A. R., Jones M. H., Motch C., 1989, MNRAS, 237, 299
Whitehurst R., 1988, MNRAS, 233, 529
Wynn G. A., King A. R., 1995, MNRAS, 275, 9